A local circuit topology for inductive parasitics[*]

Andrea Pacelli
Department of Electrical and Computer Engineering
State University of New York at Stony Brook
Stony Brook, NY 11794-2350
ap@ieee.org

ABSTRACT

A novel circuit topology for inductive coupling between interconnecting wires is presented. The model is local, i.e., only coupling between neighboring wires is explicitly modeled. However, the topology accounts for long-range coupling by propagating the vector potential from one wire to the next. Examples of model calibration, both directly from layout and as model-order reduction of a given inductance matrix, are presented for simple wiring structures.

1. INTRODUCTION

Computer-aided design of gigahertz-range digital and analog integrated circuits requires accurate and efficient models for inductive effects in interconnection wires, both on- and off-chip. Unlike capacitances and resistances, parasitic inductances do not lend themselves to simple models for circuit simulation. In the absence of magnetic materials or extensive shielding, magnetic fields propagate to large distances, with only a $1/r$ attenuation. Therefore, the coupling between numerous circuit elements must be accounted for. In mathematical terms, a *partial inductance matrix* can be defined, where each entry describes the electromotive force on a wire segment caused by the time dependence of current in another wire. Unlike the capacitance matrix, the inductance matrix is dense, i.e., in general no entries are so small as to be neglected without loss of accuracy. Moreover, the simple pruning of small elements in the partial inductance matrix may lead to unphysical and unstable networks [1]. For circuits of realistic size, the number of inductive coupling coefficients rapidly becomes unmanageable. Some attempts towards sparsifiying the inductance matrix have focused on removing long-range interactions while preserving stability [1, 2, 3]. Clearly, if such long-range interactions are important, a loss of accuracy occurs. The inductance problem may also be recast in an alternative form, by computing the inverse inductance matrix which has better sparseness and stability properties [4, 5]. Other authors have focused on algorithms to identify current-return paths [6, 7], or on multipole expansions to reduce the number of coupling coefficients [8].

Ultimately, the complexity of the existing inductance models can be attributed to the integral representation adopted, whereby the magnetic field or vector potential at any given point depends on the currents at every other point in the circuit. In this paper we present an alternative representation, which is intrinsically sparse and local. By analogy with the electrostatic problem, a vector-potential equivalent circuit (VPEC) is obtained, which describes the propagation of the vector potential from one region of space to the next. Only coupling coefficients between neighboring wires are needed, rather than between every possible pair of wires.

The model parameters can be directly extracted from wire geometry, by integration of the basic magnetostatic equations. However, the VPEC topology can also be used as a reduced-order model to recast any existing inductance matrix into a local, more sparse form, while conserving a straightforward physical interpretation for all circuit elements. With respect to alternative sparsification techniques, the present approach offers advantages of improved flexibility in the accuracy-complexity tradeoff, simplicity of implementation, and a clearer physical foundation. In this paper we mainly focus on the problem of long-range inductive interactions between large wires. Short-range phenomena such as the skin effect affect local wire models only, and can be added *a posteriori* using one of the common modeling techniques [9].

The paper proceeds as follows. In Section 2 the mathematical formalism for the vector potential in the Coulomb gauge is briefly reviewed. Section 3 introduces the topology of the VPEC. In Section 4 we describe the first-principle extraction of circuit elements from wire geometry. The unconditional stability of the equivalent circuit is proved in Section 5. In Section 6 we present examples of direct model extraction from wire geometry, while in Section 7 an example of model-order reduction is discussed. Conclusions are drawn in Section 8.

2. VECTOR POTENTIAL FORMALISM

The vector potential concept represents a convenient way of dealing with magnetostatic problems in an electrostatic-like formalism. The vector potential $\mathbf{A}$ in the Coulomb gauge is defined by [10]

$$\nabla \times \mathbf{A} = \mathbf{B} \tag{1}$$

$$\nabla \cdot \mathbf{A} = 0, \tag{2}$$

where $\mathbf{B}$ is the magnetic field. The total electric field acting on charged particles can be obtained as

$$\mathbf{E} = -\nabla\phi - \dot{\mathbf{A}}, \tag{3}$$

where the dot represents the time derivative. The three components A_x, A_y, A_z of the vector potential $\mathbf{A}$ are obtained from the three equations

$$\nabla^2 A_i + \mu J_i = 0, \qquad i = x, y, z. \tag{4}$$

With the boundary condition $\mathbf{A}(\infty) = 0$, the vector potential can be explicitly obtained as

$$\mathbf{A}(\mathbf{r}) = \frac{\mu}{4\pi} \int d\mathbf{r}' \frac{\mathbf{J}}{|\mathbf{r}' - \mathbf{r}|}, \tag{5}$$

where the integral is computed over all space. Eq. (5) can be used to compute the vector potential once the currents are known. The numerical calculation of the integral can be expensive, which motivated the development of acceleration methods based on multipole expansions [11]. In the rest of this paper we will assume that such integral can be accurately evaluated at whatever point in space and whenever necessary. As we will see, the distribution of currents can be considerably simplified, and the number of evaluations required for the integral is so small that no special acceleration techniques are needed.

With the above approach, one can find all the self- and mutual inductances of a set of conductors in three-dimensional space. With n conductors, one obtains a dense matrix of n^2 coefficients. In the next section we will find a more compact formulation of the same problem, where only order $O(n)$ electrical elements are necessary.

3. VECTOR-POTENTIAL EQUIVALENT CIRCUIT TOPOLOGY

In order to derive a local equivalent circuit for the vector potential, we decompose the entire domain of interest into discrete *control volumes,* or *boxes,* of arbitrary shape, that we denote as Ω^k [12, 13]. Typically, each control volume will surround a single wire segment. Integrating Eq. (4) over volume Ω^k and applying the Gauss theorem, we obtain

$$\int_{S^k} d\mathbf{S} \cdot \nabla A_i + \mu \int_{\Omega^k} d\Omega J_i = 0,$$

where S^k is the outer surface of Ω^k. Let us now define S^{kl} as the surface separating volume Ω^k from Ω^l, so that

$$\sum_l \int_{S^{kl}} d\mathbf{S} \cdot \nabla A_i + \mu \int_{\Omega^k} d\Omega J_i = 0, \tag{6}$$

where the sum over l includes all nearest neighbors of Ω^k. Eq. (6) can be seen as the Kirchhoff current law for the vector-potential equivalent circuit of Fig. 1. The node voltages A_i^k and A_i^l represent the (suitably averaged) *i*-component of the vector potential in volumes Ω^k and Ω^l. The current source I_i^k is defined as

$$I_i^k = \mu \int_{\Omega^k} d\Omega J_i. \tag{7}$$

The surface integrals in Eq. (6) are proportional to the gradient of the vector potential on the surfaces S^{kl}. This is similar to the expression for conduction current flow through a surface S:

$$\mathbf{J} = -\sigma \int_S d\mathbf{S} \cdot \nabla\phi,$$

where σ is the conductivity, and ϕ is the electrostatic (scalar) potential. Ohmic transport is commonly represented by resistive elements. By analogy, we model the flux of the gradient of the vector
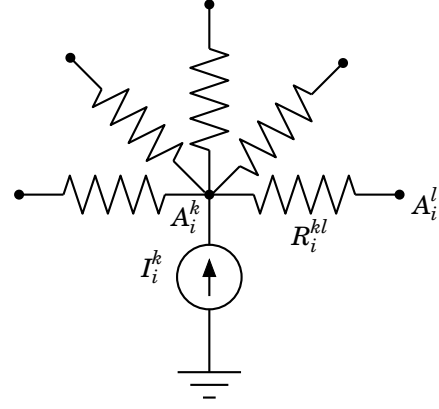

Figure 1: Equivalent circuit for the *i*-component of the vector potential A. Voltages A_i^k and A_i^l correspond to the vector potentials in two neighboring control volumes Ω^k and Ω^l. Current source I_i^k models the effect of conduction current on the vector potential. Resistor R_i^{kl} represents the propagation of vector potential between the two regions.

potential as a current flow through resistors R_i^{kl}. Since such elements do not correspond to physical resistors, they are measured not in Ohm but in units of inverse length [i.e., $1/\text{m}$ in the MKS system; see also Eq. (11) below].

The circuit of Fig. 1 has the following simple interpretation. The current source I_i^k tends to increase the *i*-component of the vector potential in region Ω^k, as shown by Eq. (5). However, the vector potential is also affected by current flowing in neighboring regions, which act through lumped resistors R_i^{kl}. Although this model is *local,* it allows for *nonlocal* effects, by letting the vector potential 'enter' and 'exit' discrete regions in space. Note that the Coulombgauge condition of Eq. (2) should not be confused with the flux equations (6). In other words,

$$\nabla \cdot \mathbf{A} = 0, \qquad \text{but} \qquad \nabla A_i \neq 0.$$

To represent the effect of the magnetic field on current flow, we must introduce a voltage source acting on charged particles. The applied voltage must be proportional to the line integral of the electromotive force:

$$V_{em}^{kl} = -\int_{\Gamma^{kl}} d\Gamma \cdot \dot{\mathbf{A}} \tag{8}$$

where Γ^{kl} is a path connecting regions k and l. In the case of narrow, rectilinear wires, with a small cross-section, the ambiguity in the choice of the integration path is usually irrelevant. Note that the straightforward use of Eq. (8) would require knowledge of the electromotive force at the interface *between* regions, to properly model conduction-current flow. However, the electromotive force is proportional to the time derivative of the vector potential, and is best defined *within* each region. It is convenient in practice to adopt two complementary discretization schemes, one for the electrical quantities (scalar potential) and another for the magnetic quantities (vector potential). When obtaining circuit equations, the edges of the electrical network will correspond to nodes for the magnetic network, and vice versa. Such staggered discretization is well known in the context of partial-element equivalent circuit (PEEC) models [14]. Accordingly, in the following we will denote the electromo-
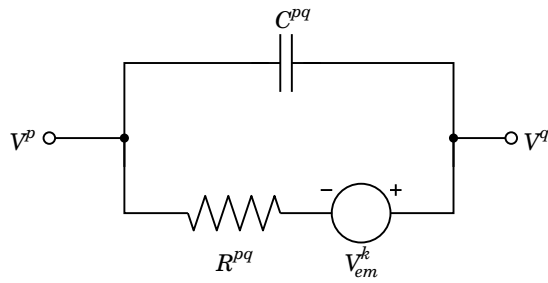
Figure 2: Equivalent circuit connecting two voltage nodes, V^p and V^q. A conventional resistor R^{pq} and capacitor C^{pq} represent the flow of conduction and displacement current between points p and q, respectively. The effect of magnetic fields is modeled by a voltage source V_{em}^k, controlled by the vector potential in the control volume Ω^k which lies between p and q.

tive voltage source as V_{em}^k rather than V_{em}^{kl}, and define it as

$$V_{em}^k = -\int_{\Gamma^k} d\Gamma \cdot \dot{\mathbf{A}} \qquad (9)$$

where Γ^k is a path internal to control volume Ω^k. The complete circuit connecting two voltage nodes, V^p and V^q, is presented in Fig. 2. The magnetic control volume Ω^k is assumed to lie in the space between points p and q. An ohmic resistance R^{pq} and a capacitance C^{pq} are shown, as well as the electromotive force V_{em}^k. Note that the topology is such that the presence of V_{em}^k does not affect the dielectric displacement represented by capacitor C^{pq}, which is proportional to the gradient of the scalar (electrostatic) potential only. However, the conduction current will be affected by the sum of the potential drop $V^p - V^q$ and the electromotive force V_{em}^k, consistently with Eq. (3).

Three circuits of the type of Fig. 1 will be defined for each volume Ω^k, one for each of the components $i = x, y, z$. If all currents are flowing in a plane (e.g., for large planar layouts, where the z dimension is negligible), then one of the circuits can be omitted. Figure 3 shows the complete circuit topology for a set of wires arranged in both x and y directions, adopting the staggered discretization scheme. Two VPECs model the x and y components of the vector potential, respectively, with resistors connecting only neighboring wires. Note that orthogonal wires do not couple magnetically. Although in this example only horizontal and vertical wires are shown, the treatment could be easily extended to diagonal wires and non-Manhattan layouts. This would be achieved by letting current in one wire affect both x and y components of the vector potential, and by letting both components of the vector potential affect the current in the wire. Boundary conditions (shown as resistors to ground) will be discussed in the next section.

4. EXTRACTION OF MODEL PARAMETERS

In the previous section, an equivalent circuit topology was rigorously obtained from field equations. However, to achieve a usable model, branch-constitutive equations are needed, whereby the currents flowing through elements are computed as functions of the terminal voltages. As will be seen later in this section, the only nontrivial parameters in the VPEC are the resistances R_i^{kl}. The number of such parameters is equal to the number of nearest-neighbor interconnections, which is of the same order of the number of physical
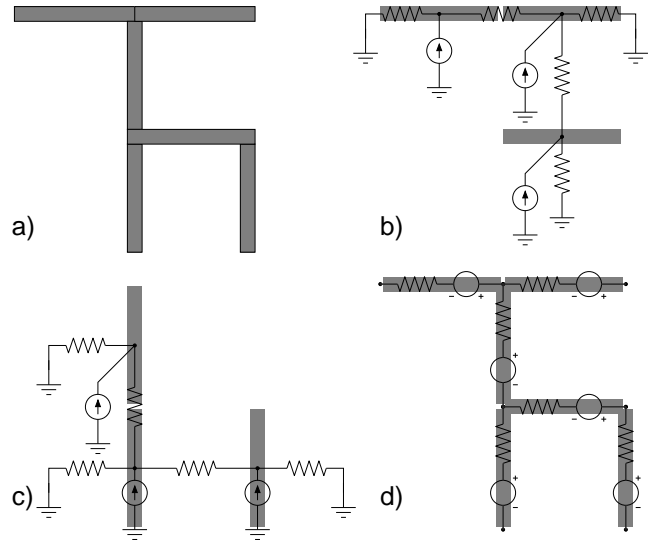

Figure 3: Complete circuit topology for a simple arrangement of wires, neglecting current conduction in the z direction. a) Physical layout (top view in the xy plane). b) Magnetic circuit for the x component of the vector potential (voltage nodes correspond to wire midpoints). c) Magnetic circuit for the y component of the vector potential. d) Electrical circuit (voltage nodes correspond to joints between wires). Wire-to-wire stray capacitances are omitted for clarity. Current sources in the magnetic circuit are controlled by currents in the electrical circuit according to Eq. (7). Voltage sources in the electric circuit are controlled by voltages in the magnetic circuit according to Eq. (9).

elements in the circuits. We will first describe how such resistors can be extracted from wire geometry. In Section 7 we will give an example of the extraction of the magnetic resistances from a precomputed, dense partial inductance matrix.

As shown in our previous paper [12], the numerical values of a physically-based equivalent circuit can be calibrated using data from numerical simulations. In this case, all the element values can be estimated from the knowledge of the current density $\mathbf{J}$. We call this initial information a 'trial' or 'experiment' and denote it by $\bar{\mathbf{J}}$. One way of obtaining a realistic current density is by a numerical solution of the Poisson and continuity equations at steady state. However, as will be shown in the following, in most practical cases an ad-hoc current density can be generated that allows a much faster evaluation of the numerical expressions.

4.1 Vector-potential resistances

First of all, let us define the average vector potential in region k as

$$A_i^k = \frac{1}{\Omega^k} \int_{\Omega^k} d\mathbf{r} \, A_i(\mathbf{r}) \, W^k(\mathbf{r}), \qquad i = x, y, z, \qquad (10)$$

where W^k is a weighing function. The weighing may be uniform ($W^k = 1$), impulsive ($W^k = \Omega^k \delta(\mathbf{r} - \mathbf{r}^k)$), or somewhere in between. Choice of weighing will be dictated by the problem at hand. The vector-potential resistance R_i^{kl} is then obtained as

$$R_i^{kl} = \frac{\overline{A}_i^l - \overline{A}_i^k}{\int_{S^{kl}} d\mathbf{S} \cdot \nabla \overline{A}_i}, \qquad (11)$$

where $\overline{\mathbf{A}}$ is the vector potential computed from a trial current distribution $\overline{\mathbf{J}}$ according to Eq. (5). Note that in principle, we do not need the current distribution $\overline{\mathbf{J}}$ to satisfy any particular property. In the case of narrow rectilinear conductors, one can simply assume a uniform current density, and force a unit current through one of the regions involved (Ω^k or Ω^l), leaving zero current in all other regions. Although unphysical ($\nabla \cdot \overline{\mathbf{J}} \neq 0!$), this situation allows the maximum accuracy in the determination of the resistance R_i^{kl}, as it emphasizes the role of the vector potentials in regions k and l and their magnetic coupling. Note that in this case, the method allows an extremely rapid model extraction, since the integral of Eq. (5) only includes volumes Ω^k and Ω^l rather than the entire simulation domain. Moreover, if the conductors are rectilinear, the surface integral in Eq. (11) can be analytically evaluated, or well approximated, in many important cases (e.g., flat and cylindrical region boundaries).

4.2 Vector-potential current sources

The current source I_i^k was defined in Eq. (7) as a function of the three-dimensional current distribution $\mathbf{J}$. If, as is typical, each volume Ω^k comprises a single wire, a unique conduction current I^k can be defined (neglecting charge storage in the wire) and the vector-potential current source is written as

$$I_i^k = F_i^k I^k,$$

where the 'current gain' F_i^k is extracted from the trial current as

$$F_i^k = \mu \frac{\int_{\Omega^k} d\Omega \overline{J}_i}{\int_{S^k} d\mathbf{S} \cdot \overline{\mathbf{J}}} \qquad (12)$$

and S^k is an arbitrary cross-sectional surface of Ω^k. If the wires are narrow and rectilinear, the calculation of the coefficient F_i^k is trivial:

$$F_i^k = \mu \hat{\lambda}_k \mathbf{u}_k \cdot \mathbf{u}_i, \qquad (13)$$

where λ_k is the conductor length, $\mathbf{u}_k$ is the unit vector giving its direction, and $\mathbf{u}_i$ is the unit vector corresponding to the i-component.

4.3 Electromotive voltage sources

Once the vector-potential circuit definition is complete, Eq. (6) becomes the Kirchoff current law

$$\sum_l \frac{A_i^l - A_i^k}{R_i^{kl}} + I_i^k = 0.$$

From the knowledge of the average vector potential $\mathbf{A}^k$ in each volume Ω^k, one can now obtain the electromotive force. If the magnetic 'voltage nodes' are defined on the edges of the electrical network, the induced voltage is computed as

$$V_{em}^k = -\sum_{i=x,y,z} E_i^k \dot{A}_i^k,$$

where the 'voltage gain' E_i^k is extracted from the trial current as

$$E_i^k = \frac{\int_{\Gamma^k} dx_i \overline{A}_i}{\overline{A}_i^k}. \qquad (14)$$

In the case of narrow, uniform, rectilinear wires, with uniform weighing of vector potential, the coefficient E_i^k reduces to

$$E_i^k = \lambda_k \mathbf{u}_k \cdot \mathbf{u}_i. \qquad (15)$$

4.4 Boundary conditions

A common issue with magnetostatic problems is that of boundary conditions. In the absence of magnetic materials, magnetic field lines slowly decay to infinity, without sources or sinks. The vector-potential approach of Eq. (5) is not affected by such problems, as it allows the calculation of the vector potential in a limited domain as long as currents are limited in space.

The extraction technique can naturally include boundary conditions. One can think of surrounding the simulation domain with extremely large regions of space, which act as grounding terminals. The average vector potential inside each of those regions is clearly zero. The resistance from region k to ground terminal 0 is then defined as

$$R_i^{k0} = -\frac{\overline{A}_i^k}{\int_{S^{k0}} d\mathbf{S} \cdot \overline{\nabla A}_i}. \qquad (16)$$

Resistance R_i^{k0} then describes the loss of vector potential into empty space and roughly plays the role of a 'vacuum impedance.' Note that such resistors act as absorbing, or perfectly-matched boundaries. Therefore, they can be placed adjacent to the wire control volumes, thus removing the need of discretizing the space around the circuit and greatly reducing model complexity.

5. STABILITY

For the VPEC to be stable, the partial-inductance matrix must be positive definite. We will prove the stability of the model for a network of narrow, rectilinear wires. The stability for more complicated geometries follows if one decomposes conductors into narrow filaments. From the model construction, the inductive effect is modeled in three steps: (1) Current flow in wire k causes injection of current into the VPEC, with current gain F_i^k. (2) As a consequence, a change of vector potential occurs at every other wire l. (3) The change of vector potential A_i^l causes an electromotive force at wire l, with voltage gain E_i^l. Therefore, the partial-inductance matrix can be written as

$$L_{lk} = \sum_{i=x,y,z} F_i^k Z_i^{lk} E_i^l = \sum_{i=x,y,z} \mu \lambda_l \lambda_k (\mathbf{u}_l \cdot \mathbf{u}_i)(\mathbf{u}_k \cdot \mathbf{u}_i) Z_i^{lk}$$

where Z_i^{lk} is the resistance matrix which describes the increase of the i-component of vector potential at node l due to a unit current injected into the VPEC at node k. It is well known that the resistance matrix of any network of positive-valued resistors is always positive definite, or else the network could generate power. From elementary matrix algebra, one sees that the positive definiteness of Z_i^{lk} guarantees the positive definitess of L_{lk}, and therefore the stability of the circuit. The adoption of a resistive network to represent the propagation of the vector potential allows not only a compact representation, but an unconditionally stable one.

6. EXAMPLES

We first illustrate the properties of the VPEC topology using the example of a single wire, of length 1 cm and square cross-section of side $100\,\mu$m. We divide the wire into sections of equal length, and define a control volume or box around each section of wire, at a distance b from the wire. Note that b is the only free parameter in the model, and the result will depend on its value. Fig. 4 shows the geometry of a wire divided into two segments, and the corresponding electric and magnetic circuits. Since the current flows only in one direction, a single component of the vector potential has to be accounted for. Current-controlled current sources feed the magnetic

circuit, which represents the propagation of the vector potential between wire segments. Voltage-controlled voltage sources feed the electrical circuit with information from the VPEC.

The parameters of the VPEC were extracted for each wire segment. The segments were approximated as lines of zero width, thus reducing Eq. (5) to a line integral. In most cases, the vector potential tends to be a slowly varying function, so that the error is very limited. An exception was made for the vector potential due to the current in a wire on the wire itself, which diverges for a wire of zero width. For that case, the classic formula of Rosa was employed for the self-inductance [15]:

$$L_{kk} = \frac{\mu \lambda_k}{2\pi} \left[\ln\left(\frac{2\lambda_k}{w_k t_k}\right) + 0.5 + 0.2235 \frac{w_k + t_k}{\lambda_k} \right],$$

where w_k and t_k are the wire width and thickness, respectively. Assuming uniform weighing within the wire volume, the average vector potential A_i^k on the wire was extracted from the self-inductance as

$$A_i^k = \frac{L_{kk}}{\lambda_k} I^k \mathbf{u}_i \cdot \mathbf{u}_k.$$

The only free parameter in the model is the size b of the control box surrounding each wire. If b is very small, the coupling resistance becomes large, and all vector potential is assumed to be 'lost' to infinity. If b is too large, the coupling between neighboring wire sections becomes too strong. It is intuitive that the best result is obtained if the flux of the vector potential gradient is allowed to propagate equally in all directions. Figure 5 shows the inductance as obtained from a Spice simulation, as a function of the box half-size b, for two cases of a single wire segment and two segments. For a single segment, the model reduces to that of a simple inductor and the result is exact. For two segments, the exact result is obtained for $b \approx 1400 \mu$m, i.e., when the control volume is slightly longer than wider, consistently with the elongated shape of the wire. This result is qualitatively similar to that obtained with the equipotential shell technique [3].

As a more practical example, we consider a 32-line bus, with four return lines. Each wire is 1000μm long, 2μm thick and 1μm wide, with a spacing of 1μm. Values of wire resistances and wire-to-wire capacitances were extracted from the wire geometry and material properties. Copper and low-κ ($\kappa = 3$) were assumed as metal and insulator, respectively. Wires were modeled using a Π topology, with capacitors connected to the ends of each segment. A driver resistance of 100Ω and load capacitance of $2\,$fF were accounted for. For the VPEC, a cell was associated with each wire segment, linked to its neighbors and to 'vector-potential ground' by resistors (Fig. 6). Experiments have shown that the use of multiple segments for each wire did not improve accuracy greatly, therefore all results refer to a single-lump model. Since all cells are identical, the evaluation of only one line integral and three surface integrals (one for each face of the cell) was necessary. A box of square cross-section was chosen, with a side equal to the pitch of the bus, i.e., $b = 1 \mu$m. The square shape ensures that the propagation of vector potential from each wire is approximately isotropic. Figure 7 shows the transient response at the far end of the first two lines, as obtained from a Spice simulation, comparing a dense-matrix model with lower-order approximations. The dense partial-inductance matrix was obtained from Rosa's analytical expressions [15], which is shown to fit the result from FastHenry [11] closely. The Spice netlist obtained from the dense matrix includes 36 inductors and 630 coupling elements between them. The local model has only 71 resistors in the magnetic network (36 to ground, and 35 between wires).
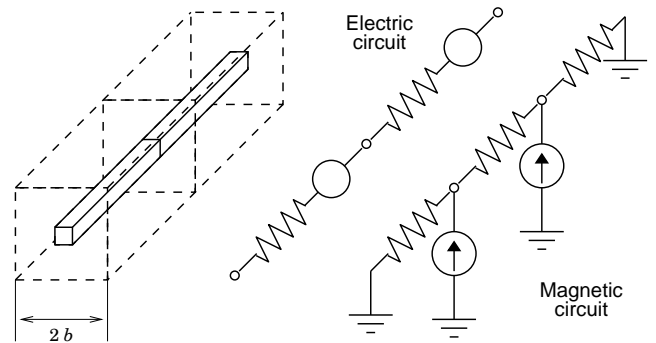

Figure 4: Geometry and equivalent circuit of an isolated single wire, divided into two segments of equal length. Each segment is surrounded by a control volume. Three voltage nodes define the electric circuit, corresponding to the voltages at the ends of each wire segment. Two vector-potential node define the magnetic circuit, corresponding to the average vector potential along each of the wire segments. Current sources feed the vector-potential circuit, while voltage sources feed back information on the vector potential into the electric circuit. Resistors in the magnetic circuit represent propagation of vector potential between wires.

Both the delay due to inductance and the amplitude of the ringing are well captured by the local model.

Figure 8 illustrates the sensitivity of the model with respect to the vertical box half-size b. Note that in this case, the cross-section of the control volumes is rectangular, with the horizontal side equal to the pitch of the bus, and the vertical side equal to $2b$. The same result of Fig. 7 is shown, where b is varied between 0.5μm and 2μm. When b is made very small, coupling between integration boxes is negligible. The figure shows that in that case, the result approaches that obtained from an *RLC* model, where only the self-inductance of each wire is accounted for (i.e., when the coupling elements are omitted). Such a model fails to reproduce the overshoot on the active line, while it overestimates coupling to the quiescent line. On the other hand, when the box is made too tall, coupling is overestimated. The 50% delay, which is dominated by the wire self-inductance, is almost unaffected. The sensitivity of the initial overshoot is around $\pm 10\%$ for a factor-of-four variation in b.

7. MODEL-ORDER REDUCTION

In Section 4 we have discussed how to directly extract model parameters from wire geometries. However, the VPEC topology can also be used as a model whose parameters are fitted to external simulations or measurements, or as a reduced-order model, to approximate a dense partial-inductance matrix. This procedure allows one to achieve a guaranteed accuracy, which is arbitrarily close to the one of the dense inductance matrix. It can be shown that, in general, a choice of model parameters can be found that conserves a number of elements in the partial-inductance matrix equal to the number of parameters in the model, i.e., the number of nearest neighbors in the topology. Therefore, a VPEC where all wires are coupled can exactly reproduce any given partial-inductance matrix. Here we will only show preliminary results for a very simple case, saving a full discussion of the order-reduction algorithm and its applications for a forthcoming publication.
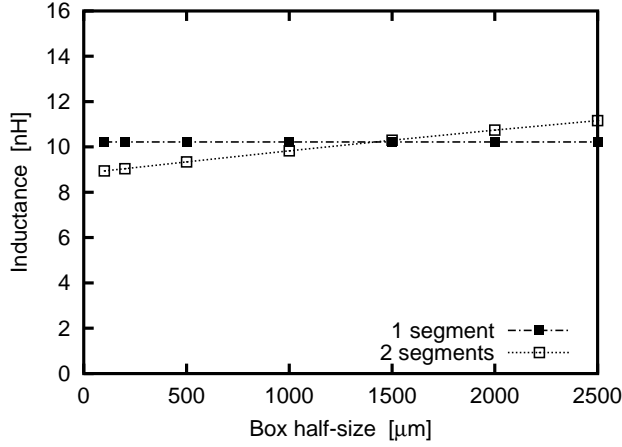
Figure 5: Self-inductance of a wire of length 1 cm and square cross section of 100μm side. The results are plotted as a function of the half-size of the control volume enclosing each wire segment. A one-segment model (solid squares) always yields the correct self-inductance, while the two-segment model (open squares) displays some sensitivity on the size of the control volume.
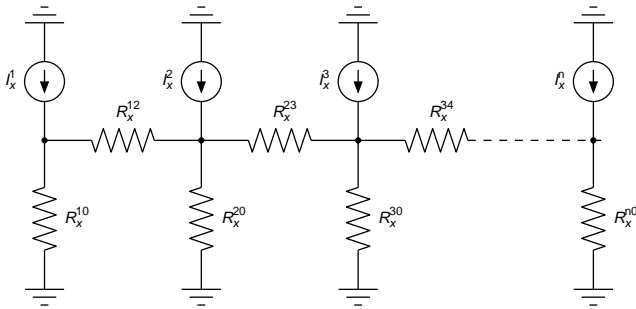

Figure 6: Vector-potential circuit for a bus with n lines. Since all lines are parallel to the x directions, all elements are labeled with the subscript x. The current-controlled current sources I_x^k feed the circuit with information from the electrical currents flowing in each wire. Resistors R_x^{k0} and $R_x^{k,k+1}$ couple each wire to 'vector-potential ground' (i.e., vacuum) and to its right-hand neighbor, respectively.

We consider three parallel wires, with parameters identical to the preceding example. We generated three different models, all with the same topology of Fig. 6 but using the resistances as free parameters to conserve a given set of partial inductances. The first model exactly conserves all self-inductances and all nearest-neighbor partial inductances, i.e., L_{kk} and $L_{k,k+1}$. The second model conserves all partial inductances from the first line to the other two lines, i.e., L_{1k}. Finally, the third model conserves the partial inductances from the third line to the other two lines, i.e., L_{3k}. The three models are compared in Fig. 9, where the response on the middle line is shown when a step is applied to the first line. The first model yields a very close approximation to the full partial-inductance response. The third model, as expected, departs from the exact result, because the interaction between first and second line was not given any importance. However, also the second model, where L_{12} was exactly
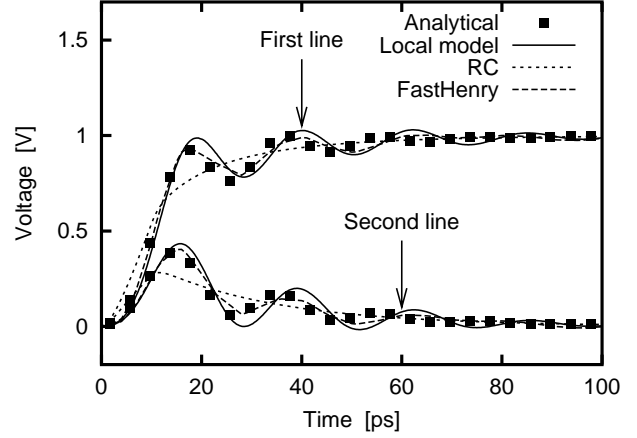

Figure 7: Transient response of the first two lines in a 32-bit bus with four return lines. A 1-V step with rise time of 10 ps was applied to the first line. The output voltage is shown at the far end of the lines. Results are reported for the dense inductance matrix using Rosa's analytical formulas, the same matrix obtained from FastHenry, the vector-potential local model, and an *RC*-only model. The FastHenry simulation included 9 filaments per wire, to model the skin effect.
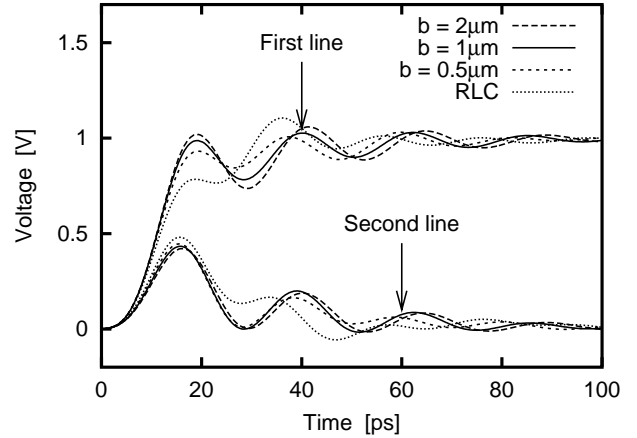

Figure 8: The transient response of Fig. 7, for different values of the control volume half-size b. The *RLC* (self-inductance only) result is also reported for reference.

conserved, shows some error, due to the neglect of the coupling between the second and third lines. In general, the first-principle methods described in Section 4 and the model-order reduction technique give comparable results, if properly applied (i.e., using physically sound control volumes in the first case, and fitting appropriate nearest-neighbor couplings in the second).

The VPEC topology can be recalibrated to fit an arbitrary subset of any given partial-inductance matrix. This property is similar to other sparsification techniques. For example, the equipotential-shell method conserves all loop inductances within a given region of space, while truncating all long-range interactions [3]. The topology presented in this paper promises a greater flexibility, be-
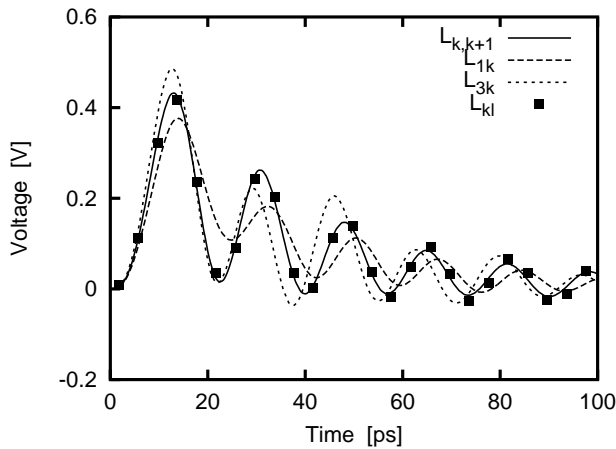
Figure 9: Transient response at the middle line of an array of 3 parallel wires, when a step of 1 V is applied to the first line. Material parameters are identical to the examples of Figs. 7 and 8. Three models are compared, obtained as model-order reduction of the dense partial-inductance matrix (L_{kl}) and conserving the nearest-neighbor inductance ($L_{k,k+1}$) and the inductances from the first (L_{1k}) and third (L_{3k}) lines.

cause if necessary, even long-range couplings can be conserved, independently from the physical arrangement of wires. A full inductance-extraction environment, which offers a wide range of modeling and order-reduction options, is currently under development.

8. CONCLUSIONS

We have presented a novel circuit topology for the description of inductive effects in interconnection wires. The topology is intrinsically local, so that the number of coupling coefficients is of the same order of the number of wires in the circuit, rather than quadratic as in the inductance-matrix approach. The model parameters can be extracted from layout, or obtained by model reduction from a given partial-inductance matrix. Initial experiments have shown that this approach allows a unique flexibility in the accuracy-complexity tradeoff.

ACKNOWLEDGMENT

REFERENCES

[1] B. Krauter and L. T. Pileggi, "Generating sparse partial inductance matrices with guaranteed stability", in *Proc. International Conference on Computer-Aided Design*, 1995, pp. 45–52.

[2] K. Shepard and Z. Tian, "Return-limited inductances: A practical approach to on-chip inductance extraction", *IEEE Trans. Computer Aided Design of Integrated Circuits and Systems*, vol. 19, pp. 425–436, 2000.

[3] M. Beattie, B. Krauter, L. Alatan, and L. Pileggi, "Equipotential shells for efficient inductance extraction", *IEEE Trans. Computer Aided Design of Integrated Circuits and Systems*, vol. 20, pp. 70–79, 2001.

[4] A. Devgan, H. Ji, and W. Dai, "How to efficiently capture on-chip inductance effects: Introducing a new circuit element *K*", in *Proc. IEEE/ACM International Conference on Computer Aided Design*, 2000, pp. 150 –155.

[5] M. Beattie and L. Pileggi, "Efficient inductance extraction via windowing", in *Proc. Design, Automation and Test in Europe*, 2001, pp. 430–436.

[6] B. Krauter and S. Mehrotra, "Layout based frequency dependent inductance and resistance extraction for on-chip interconnect timing analysis", in *Proc. Design Automation Conference*, 1998, pp. 303–308.

[7] S. Lin, N. Chang, and S. Nakagawa, "Quick on-chip self- and mutual-inductance screen", in *Proc. Intl. Symposium on Quality Electronic Design*, 2000, pp. 513–520.

[8] M. Beattie, S. Gupta, and L. Pileggi, "Hierarchical interconnect circuit models", in *Proc. International Conference on Computer Aided Design*, 2000, pp. 215 –221.

[9] H. A. Wheeler, "Formulas for the skin effect", *Proc. IRE*, vol. 30, pp. 412–424, Sept. 1942.

[10] J. D. Jackson, *Classical Electrodynamics*, John Wiley and Sons, 1975.

[11] M. Kamon, M. Tsuk, and J. White, "FASTHENRY: A multipole-accelerated 3-D inductance extraction program", *IEEE Trans. Microwave Theory and Techniques*, vol. 42, pp. 1750–1758, Sept. 1994.

[12] A. Pacelli, M. Mastrapasqua, and S. Luryi, "Generation of equivalent circuits from physics-based device simulation", *IEEE Trans. Computer Aided Design of Integrated Circuits*, vol. 19, pp. 1241–1250, Nov. 2000.

[13] S. Luryi and A. Pacelli, "Automatic generation of RF compact models from device simulation", in *Proc. Fifth International Conference on Modeling and Simulation of Microsystems*, San Juan, PR, Apr. 2002, pp. 702–709.

[14] A. E. Ruehli, "Equivalent circuit models for three-dimensional multiconductor systems", *IEEE Trans. Microwave Theory and Techniques*, vol. 22, pp. 216–221, Mar. 1974.

[15] E. B. Rosa, "The self and mutual inductances of linear conductors", *Bulletin of the Bureau of Standards*, vol. 4, pp. 301–344, Jan. 1908.